Statistical Discrimination Index Founded on Rate of Change of Phase Angle for Immunization of Transformer Differential Protection Against Inrush Current

Electrical Power and Energy Systems 134 (2022) 107381

Contents lists available at ScienceDirect

International Journal of Electrical Power and Energy Systems

journal homepage: www.elsevier.com/locate/ijepes

Statistical discrimination index founded on rate of change of phase angle for immunization of transformer differential protection against inrush current

Haidar Samet [a,b,*], Maral Shadaei [c], Mohsen Tajdinian [a]

[a] Department of Power and Control Engineering, School of Electrical and Computer Engineering, Shiraz University, Shiraz, Iran
[b] Department of Electrical Engineering, Eindhoven University of Technology, Eindhoven, the Netherlands
[c] Fars Power Maintenance Company, Shiraz, Iran

ARTICLE INFO

Keywords:
Differential Protection
Transformer Inrush Current
Internal Fault
Standard Deviation

ABSTRACT

Magnetizing inrush currents are known as the most critical potential threat in maloperation of the transformer differential protection. Therefore, there is a need to detect the inrush current from the internal fault current to avoid the differential protection maloperation. Due to the possibility of a current transformer (CT) saturation at a high level of inrush and fault current, the discrimination algorithm should function appropriately in CT saturation conditions. Here, a method is developed based on the rate of phase angle change (RoCoPA) to perform the discrimination process. The proposed discrimination index employs the RoCoPA of the three-phase differential currents and calculates the standard deviations of the RoCoPA of the three-phase differential currents. The discrimination procedure is designed based on the fact that during fault scenarios, the signal remains almost sinusoidal, and as a result, the RoCoPA has the minimum variations.

On the contrary, owing to the non-sinusoidal wave shape of the inrush current, the RoCoPA has notable variations. Based on the various simulated and practical scenarios, the proposed index's performance is evaluated considering challenging scenarios. The results reveal that the proposed discrimination index has promising accuracy with average response delay with about half a cycle.

1. Introduction

Power transformers play a crucial role in converting voltage levels and supplying power for power systems. Differential protection is one of the essential protections applied to the transformer, so it needs to operate correctly in the fault condition. During power transformer energization, a large inrush current may be created several times larger than the rated transformer current. The inrush current can impose destructive consequences such as the transformer lifecycle reduction due to high mechanical and thermal stress in windings, power quality issues, and mal-operation of the overcurrent and differential protective relays [1]-[2]. This paper concentrates on avoiding mal-operation of the differential protective relays during inrush currents.

There are many methods for distinguishing fault current from inrush current. These methods have distinguished the fault current from the inrush stream with different approaches. According to these approaches, the methods can be grouped into five categories:

Harmonic Restraint Algorithms (A1) [3]-[4]: These methods make decisions by calculating the ratios of the second and fifth harmonic components to the fundamental frequency component of the transformer differential current. The main problem with these methods is that by changing the core material of the modern transformers, the structure and ratio of the harmonics change, affecting the reliability of these methods.

Flux restrain and Inductance based Algorithms (A2) [5–7]: These methods separate the inrush current from the fault current using the transformer magnetization information and curve. The proposed methods are based on the calculation of voltage, flux, and Inductance of magnetization. Comparing with other methods, these methods have a high dependency on the transformer parameters.

Artificial Intelligence Algorithms (A3) [8–10]: These methods are implemented using neural networks and fuzzy logic. Despite the high speed of these methods, training of the neural network is required with the help of an extensive database.

* Corresponding author at: Department of Power and Control Engineering, School of Electrical and Computer Engineering, Shiraz University, Shiraz, Iran.
E-mail address: samet@shirazu.ac.ir (H. Samet).

https://doi.org/10.1016/j.ijepes.2021.107381
Received 11 February 2021; Received in revised form 28 April 2021; Accepted 13 June 2021
Available online 10 July 2021

Table 1
Qualitative Comparison Between The State-Of-The-Art Algorithms.

Algorithms	Data Requirement	Computational Burden	Noise Sensitivity	CT Saturation
A1	1 Cycle	Moderate	Low	Venerable
A2	Up to 1 Cycle	High	Low	Relatively Immune
A3	Up to 1 Cycle	Very High	Moderate	Relatively Immune
A4	Up to 1 Cycle	Moderate	Very High	Relatively Immune
A5	Up to 1 Cycle	Relatively Low	Moderate	Immune

Time-Frequency Based Algorithms (A4) [11–15]: These methods extract and characterize specific signal features in the frequency or time domain and help make decisions. However, high-sampling rate and noise sensitivity are known as the main challenges of these methods.

Hybrid and Innovative Algorithms (A5) [16–25]: This category includes tasks similar to the nature of the signal analysis. In [19], by calculating the center of gravity of the signal in the time domain and in [20] by calculating the signal similarity to the sinusoidal waveform, the fault current is subtracted from the inrush current. In [21], the inrush current is detected by calculating the kurtosis of the signal. Besides, [22] identifies the current as inrush current by providing indicators for the three phases of the current if the indicators for all three phases are violated. In [23], the authors presented a differential protection scheme based on the voltage and current signals. While this method discriminates internal fault and inrush current, the calculation based on the discrete Fourier transform may impose some delays, especially during internal fault accompanied by CT saturation.

In the following, Table 1 provides a qualitative comparison between the state-of-the-art algorithms. As it can be seen in Table 1, harmonic restrain algorithms have at least one cycle delay with vulnerability against identification during hard cases (i.e., CT saturation and inrush current with high remanent flux). Except for harmonic restrain algorithms, other algorithms can identify that the inrush current is less than one cycle (considering the mathematical tools). Comparing to all algorithms, the computational burden of hybrid algorithms is relatively low. This is because these algorithms are mostly designed based on simple mathematic to extract features from standard fault current signal (i.e., the combination of a sinusoidal component and a DC offset component). Between all algorithms, time–frequency-based algorithms have a high sampling rate, and they have noise sensitivity more than other algorithms. Eventually, comparing all algorithms, hybrid algorithms have successfully achieved CT saturation immunity more than other algorithms, thanks to utilizing unsaturated interval data and waveform reconstruction.

Nevertheless, comparison of the previously suggested algorithms indicates that dealing with internal fault accompanied with CT saturation, inrush current with internal fault, inrush current in the presence of high remanent flux in less than cycle (i.e., sub-cycle) with low-computational burden and immunity to other sources of interference such as noisy condition can still be considered as the potential motivations for working on the efficient algorithm.

In this paper, a new method is proposed using the concept of RoCoPA to distinguish inrush current from fault current. The proposed method makes a decision by calculating the standard deviation of the RoCoPA of the differential current in several consecutive samples of data. The RoCoPA calculated from the fault current, due to being present in the linear region of the transformer saturation curve in the consecutive samples, has an almost constant value. However, in the case of the inrush current, because of the transformer saturation, we will see the nonlinear behavior of the transformer [26]. This will result in large fluctuations in the RoCoPA extracted from the transformer differential waveform in the case of inrush current. Finally, as the standard deviation of the RoCoPA is greater than the specified threshold, the event is diagnosed as an inrush current in successive samples. Also, unlike [22], the proposed algorithm performs well in CT saturation conditions without additional criterion.

Comparing with state-of-the-art algorithms given in Table 1, the proposed method requires sub-cycle data for decision making. The proposed method is also designed based on the practical and low-complex mathematical tool called least mean squares, leading to a computational burden method. However, the nature of the proposed method is designed so that it calculates the RoCoPA based on the least mean squares (LMS), and as a result, it has inherent noise immunity. The proposed algorithm has immunity against challenging scenarios, including CT saturation and recognizing the minor internal fault scenarios.

It should be noted that this algorithm operates based on the differential current. If the differential current does not trigger the relay, the signal is not considered a disturbance, and it is not fed to the discrimination algorithm. As a result, the proposed approach, which basically is a discrimination algorithm, is capable of detecting the minor fault scenario that the relay feeds into it.

The rest of the paper is constructed as follows: In Section 2, the theory of RoCoPA and the proposed method is explained. In Section 3, the simulation and experimental scenarios and results are presented. Finally, in Section 4, the conclusion is presented.

2. Proposed algorithm

The presented discrimination algorithm is established on the RoCoPA of the differential currents. More specifically, the proposed algorithm monitors the RoCoPA's variation of the differential current. As a result, it is essential to calculate the RoCoPA of the current signal. In the following, the RoCoPA is first calculated, and afterward, the proposed index is introduced.

A. Calculating RoCoPA

In general, the current signal in the power system can be represented in continuous-time form as follows:

$$i(t) = I_m \cos(\varphi(t)) + \epsilon(t) \tag{1}$$

in which I_m is the peak value of the fundamental component, $\epsilon(t)$ is the noise term, φ is the phase angle of the fundamental component. According to (1), the RoCoPA is calculated as follows:

$$RoCoPA = \frac{d(\varphi(t))}{dt} \tag{2}$$

As it can be inferred from (2), to calculate the RoCoPA, it is essential to estimate φ. Owning to the application of the proposed method, φ can be approximated by a linear function as follows:

$$\varphi(t) \approx \varphi_0 + \varphi_1 t \tag{3}$$

Substituting (3) in (2), the RoCoPA is calculated as follows:

$$RoCoPA \approx \varphi_1 \tag{4}$$

From (4), it is revealed that the RoCoPA depends on the variations of φ_1 and as a result, φ_1 should be estimated from the current signal. As a result, to obtain the RoCoPA, the current signal is expressed in discrete form as follows:

$$i(k) = I_m \cos(\varphi_0 + \varphi_1 k\Delta T) + \epsilon(k) \tag{5}$$

The expression (1) can be rewritten in complex form through the following:

$$i(k) = i(k) + ji\left(k - \frac{T}{4}\right) + \epsilon(k)$$

$$= I_m e^{j(\varphi_0 + \varphi_1 k\Delta T)} + \epsilon(k) \tag{6}$$

The aim is to estimate the RoCoPA from the following fundamental component of the current signal known as $\widehat{i}$:

$$\widehat{i}(k) = I_m e^{j(\varphi_0 + \varphi_1 k\Delta T)} \tag{7}$$

As a result, expression (7) can be written as follows:

$$i(k) = \widehat{i}(k) + \epsilon(k) \tag{8}$$

From the model given in (8), the current signal can be calculated as follows:

$$\widehat{i}(k) = \widehat{i}(k-1)e^{j\varphi_1 \Delta T} \tag{9}$$

The estimation error signal $e(k)$ is calculated as follows:

$$e(k) = i(k) - \widehat{i}(k) \tag{10}$$

in which $\widehat{i}(k)$ is the estimated model of current at the *k-th* instant, and it is expressed as follows:

$$\widehat{i}(k) = \widehat{i}(k-1)w(k) \tag{11}$$

where w(k) is the weight coefficient expressed by $w(k) = e^{j\widehat{\varphi_1}(k)\Delta T}$, and $\widehat{\varphi_1}$ is the estimated RoCoPA. As one can see in (11), the input vector contains one element and, consequently, one weight vector.

To estimate the RoCoPA, the least mean squares (LMS) algorithm is applied to the weight coefficient $w(k) = e^{j\widehat{\varphi_1}(k)\Delta T}$. The LMS algorithm recursively minimizes the squared of the error weight vector at each sampling instant as follows:

$$w(k) = w(k-1) + \mu(k)e(k)\widehat{i}^{*}(k) \tag{12}$$

where the star sign (*) denotes the complex conjugate the value and $\mu(k)$ is the convergence factor that controls the stability and rate of convergence of the algorithm.

As stated in [27], $\mu(k)$ is varied to provide better convergence of the LMS algorithm in the presence of noise. To modify the estimation, the following equation is employed:

$$\mu(k+1) = \xi\mu(k) + \chi r(k)r^{*}(k) \tag{13}$$

in which $r(k)$is the autocorrelation of $e(k)$ and $e(k-1)$ and it is computed as follows:

$$r(k) = \eta r(k-1) + (1-\eta)e(k)e(k-1) \tag{14}$$

where $\eta$is an exponential weighting parameter and varies between $0<\eta<1$, ξ ($0<\xi<1$) and $\chi > 0$ are the factors that control the convergence time. Note that if $\mu(k+1)$ crosses lower and upper boundaries, it is adjusted to μ_{max} or μ_{min}, respectively. At each sampling interval, the RoCoPA is calculated as follows:

$$\widehat{\varphi_1}(k) = \frac{\cos^{-1}(Re(w(k)))}{2\pi\Delta T} \tag{15}$$

where *Re* denotes the real part of the complex coefficient. To implement LMS for estimating the RoCoPA, the tuning factors which are adopted from [27], consist of $r(0) = 0$, η=0.99, ξ=0.97, χ=0.01, μ_{min}=0.0001 and$\mu_{max} = 0.18$.

B. Proposed Discrimination Index

In this section, the concept of RoCoPA is used to distinguish the fault current from the inrush current. As mentioned, the inrush current has a nonlinear nature due to the performance of the transform in the saturation region of its magnetic curve, so it follows the nonlinear relation. By extracting the RoCoPA of the inrush current, in the successive samples, the oscillations of the RoCoPA are large. However, due to almost sinusoidal waveform, the RoCoPA has an almost constant value during fault conditions. As a result, it can be concluded that by calculating the RoCoPA of the transformer differential current, if the standard deviation is higher than the threshold, the event specification is categorized as an inrush current. If it is lower than the threshold, it is categorized as a fault current. The standard deviation function (SDF) is calculated as follows:

$$SDF = \sqrt{\frac{1}{K-1}\sum_{k=1}^{K}\left(RoCoPA_k - \overline{RoCoPA}\right)} \tag{16}$$

where K is the number of samples in the arbitrary window of data. It should be noted that the SDF is calculated in each phase separately. The decision criterion is the maximum of the SDF of the three-phase or in abbreviated form (SF), which is expressed as follows:

$$SF = max\{SFA.SFB.SFC\} \tag{17}$$

The flowchart of the method implementation is shown in Fig. 1. As can be seen, the current of all three phases is received, and the RoCoPA of changing phases is calculated for the time ti to tj after the event detection. By calculating the standard deviation of the RoCoPA (SF) in a specified data window for changing phases (SFA, SFB, and SFC), if their maximum is greater than the threshold (TH), the event is categorized as the inrush current.

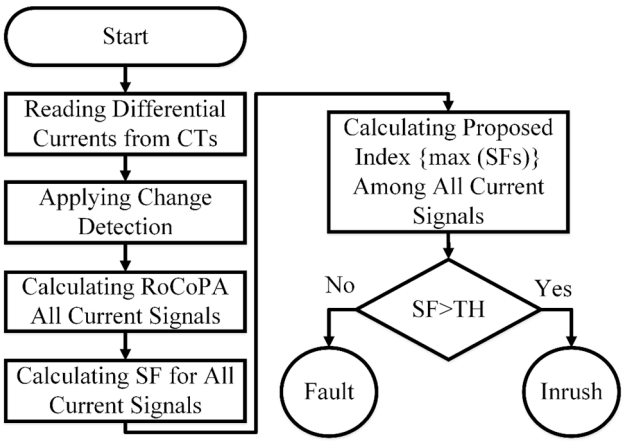

Fig. 1. Proposed algorithm implementation procedure.

Table 2
Different Threshold And Window Length For Simulated Data.

Range	Error	Delay	Gap
20–30	4.23	0.00384	–
20–40	0.704	0.00512	–
20–50	0%	0.00640	0.7764
20–60	0%	0.00768	0.3398
20–70	0.704	0.00896	–
20–80	0%	0.01024	0.2798
20–90	0%	0.0115	1.1124
20–100	0%	0.0128	1.4353
20–110	0%	0.0140	1.5187
20–120	0%	0.0153	2.2536
20–130	0%	0.0166	3.043
20–140	0%	0.0179	3.8125

C. Threshold Selection

Two crucial things in the simulation are the harmonic and the decaying DC component. Error due to low harmonic distortion percentage of fault current cannot affect simulation results. However, the decaying DC component generates more fluctuations in RoCoPA, which is solved by defining the appropriate threshold. So, it is imperative to determine the threshold and sample start and end of the calculation. For this purpose, accuracy and gap thresholding are investigated for

Table 3
Different Threshold And Window Length For Practical Data.

Range	Error	Delay	Gap
20–30	21.54	0.00384	–
20–40	16.92	0.00512	–
20–50	12.31	0.00640	–
20–60	7.69	0.00768	–
20–70	12.31	0.00896	–
20–80	0%	0.01024	18.437
20–90	0%	0.0115	1.1616
20–100	0%	0.0128	0.6879
20–110	0%	0.0140	0.3831
20–120	0%	0.0153	0.2304
20–130	0%	0.0166	0.0339

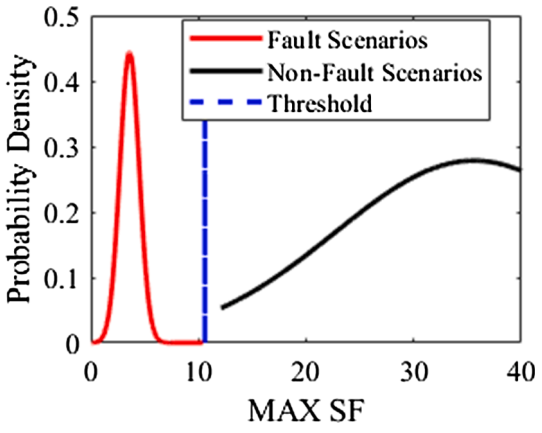

Fig. 2. PDFs for the index max SF and the selected threshold.

different window lengths, following Tables 2 and 3. The term "range" refers to the start and final samples of the calculation window (after the change detection instant) in the aforementioned tables. A sampling time of 128 μs (156 samples per cycle) is used in all scenarios. So the delay of the proposed algorithm can be calculated by multiplying the last window sample by 128 μs, which is shown in the third column of Tables 2 and 3. The Gap value is the difference between the minimum value of max(SF) in all the inrush current scenarios, and its maximum value related to all studied short circuit scenarios. Larger values of Gap reveal more accuracy of the algorithm. According to the results of Tables 2 and 3, the window, the starting and final samples equal to 20 and 90 have satisfactory results. The threshold (TH) is chosen equal to 10.6, which the center value of the gap between the worst inrush current and short circuit scenarios. Note that the threshold is independent of transformer parameters, and it only depends on the phase angle variation.

To verify the obtained threshold, an algorithm named the Otsu thresholding method was utilized, which is a well-known and reliable method employed in different engineering fields [28–30]. This technique is an effective and simple method that basically compares the difference between two or more probability density functions to provide a proper threshold. More details regarding the Otsu thresholding method are provided in [28]. As one can see in Fig. 2, the obtained threshold in Tables 1 and 2 is confirmed with the Otsu thresholding method due to the reliable distance between threshold and max (SF) of inrush current scenarios.

3. Performance evaluation and results discussion

The power system of Fig. 3 has been simulated using PSCAD to evaluate the proposed method. Fig. 3 system comprises a 400/230 kV, Yg-Δ, 500MVA transformer. The transformer models and CTs specifications are available in [16] and provided in the appendix. To study differential protection, the test system is simulated in the PSCAD. The CT model of PSCAD software is used for the simulation of CT saturation. The sampling frequency is 7.8 kHz and is equal to the sampling frequency of the laboratory data.

Different scenarios, including different fault locations in both sides of the power transformer, CT saturation and non-saturation, transformer and CT residual flux level, different angles of transformer energizing and transformer energizing with internal fault are produced in large numbers, which will be shown and described in the following:

- Inrush current
- Internal fault
- Transformer energizing with pre-existing internal fault
- Inrush current and fault current in the presence of CT saturation

Note that during simulation, the loading condition in the case of inrush current was assumed no-load condition. In contrast, in the case of

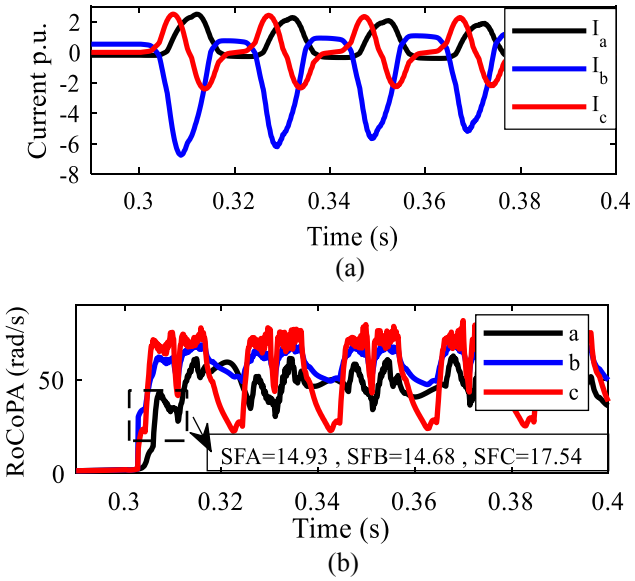

Fig. 4. Simulated inrush current waveform (a) Current, (b) RoCoPA.

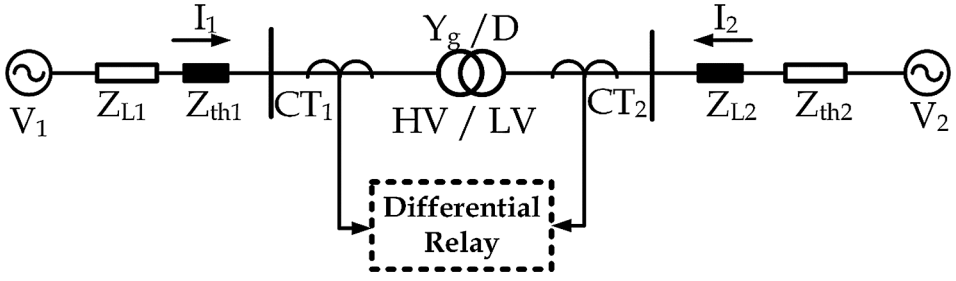

Fig. 3. A Y/D 400/230 kV transformer for simulation in a PSCAD environment.

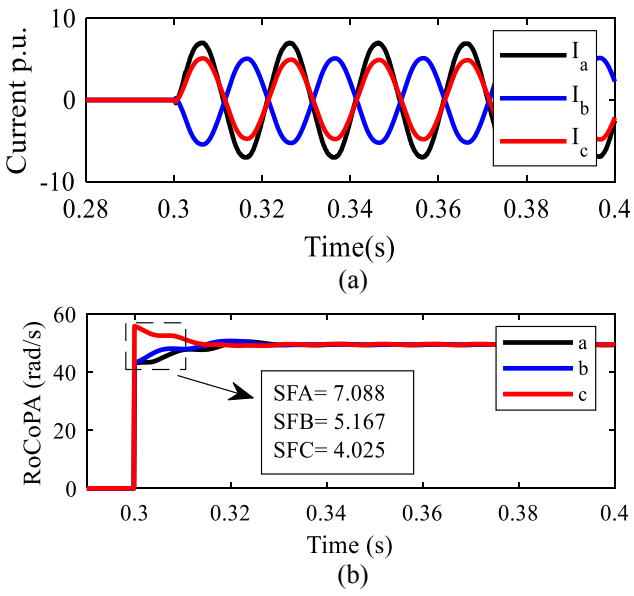

Fig. 5. Simulated fault current waveform (a) Current, (b) RoCoPA.

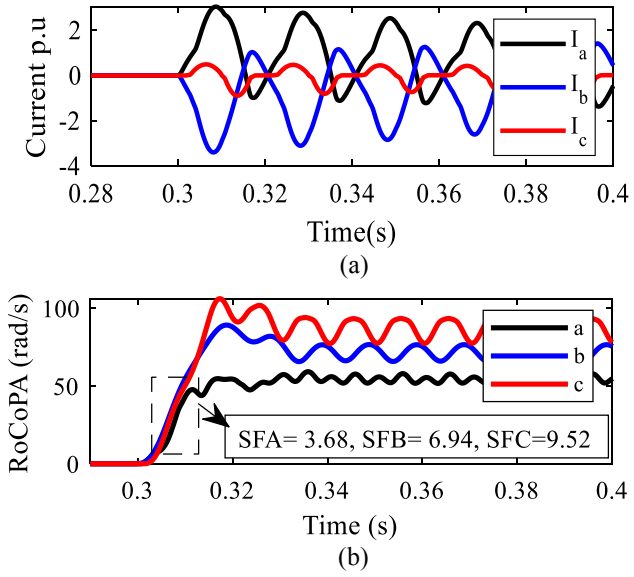

Fig. 6. Energized transformer with the internal fault (a) Current, (b) RoCoPA.

a fault condition, the transformer's loading condition varies between 50% and 100% of the nominal loading of the transformer.

A. Inrush current

This scenario involves the energizing of the transformer, with a 30% residual flux at 300 ms. As shown in Fig. 4, all three phases with different polarities are involved in the inrush current. By calculating the RoCoPA using the LMS algorithm, the RoCoPA is shown in Fig. 4. By calculating the standard deviation of the RoCoPA from 20 samples after switching to 90 samples after switching for all three phases, the values of SFA, SFB, and SFC will be as shown in Fig. 4. Their maximum is 17.54 and is above the threshold of 10.6, so this scenario is classified as an inrush current. Therefore, the classification with 90 sample delay was performed correctly at the sampling frequency of 156 samples per cycle. Note that comparing Fig. 4(a) and (b) indicates that the RoCoPA is independent of the magnitude of the inrush current.

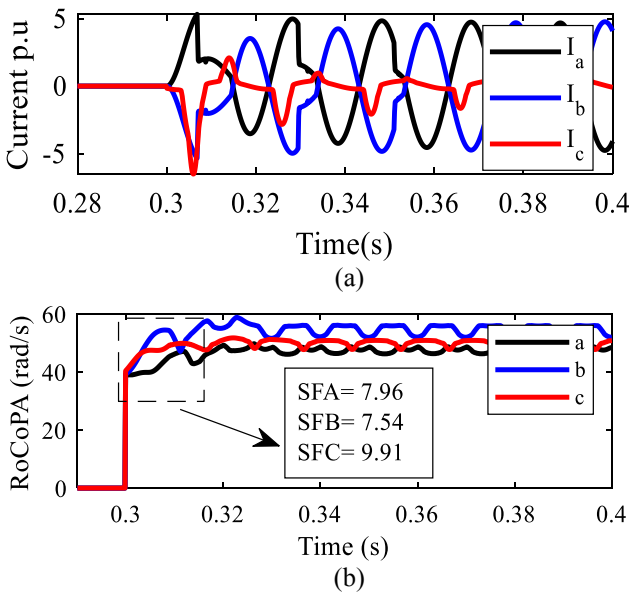

Fig. 7. Saturated fault current (a) Current, (b) RoCoPA.

B. Fault current

This scenario involves a 3-phase fault with a high impedance in the transformer terminal, so as shown in Fig. 5, we do not see the current transformer saturation. An error occurred at 300 ms. The RoCoPA is as shown in Fig. 5. As can be seen, the RoCoPA has fewer fluctuations than Fig. 5. By calculating its standard deviation for all three phases and calculating the maximum value of the standard deviation, according to Fig. 5, 7.088 obtained, it is less than the threshold of 10.6, so the event is correctly diagnosed as a fault a delay of about half cycle.

C. Transformer energizing with pre-existing internal fault

To investigate the more complicated cases, the transformer, which has an internal fault of 10% winding (a weak fault) simulated for energizing at 300 ms. As shown in Fig. 6, the currents waveform is a combination of the fault current and the inrush current. The RoCoPA will be as shown in Fig. 6. By calculating SFA, SFB, and SFC, their maximum value is 9.52, close to the threshold. However, the method has correctly identified the fault occurrence. In an internal fault with a lower level of current, the proposed method will not be able to detect an internal fault because the maximum standard deviation of the RoCoPA will be greater than the defined threshold.

D. Inrush current and fault current in the presence of CT saturation

1) Fault current

In all simulated fault scenarios in CT saturation, 98% of the simulation results were correct. However, to increase the accuracy to 100%, the reconstructed current of CT should be calculated [25] and then is fed to the RoCoPA is calculated. Fig. 7 contains the saturated fault current due to the high residual flux and fault current level. The RoCoPA is shown in Fig. 7. By calculating SFA, SFB, and SFC, all three are below the threshold, so the event is diagnosed as a fault. It is noteworthy that the operation was delayed approximately half a cycle after the change detection.

2) Internal Fault

In the inrush current scenarios in 100% of the cases where the current of CT was saturated, the correct answer was obtained, so no need to reconstruct the saturated current of CT. Fig. 8 Displays the inrush

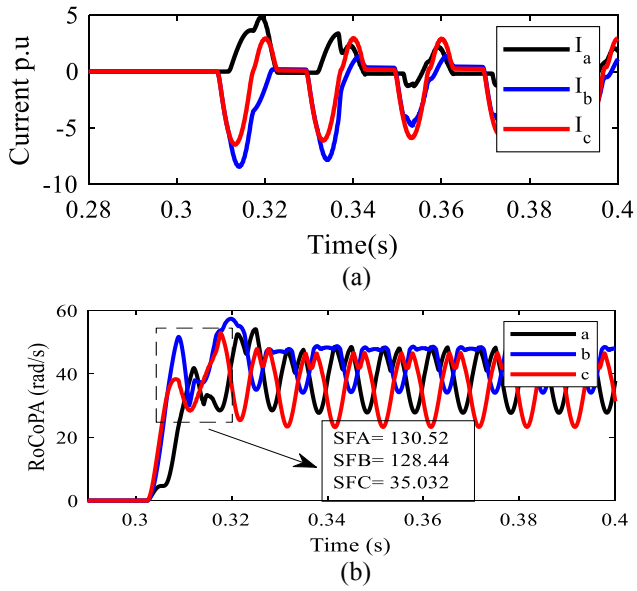

Fig. 8. Saturated inrush current (a) Current, (b) RoCoPA.

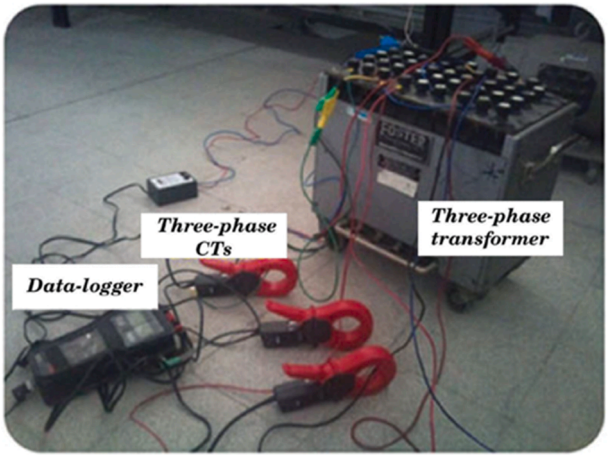

Fig. 9. Photo of a prototype transformer.

current that has saturated the CT. By calculating the SF for all three phases, the maximum SF in the three phases is 130.52, which is well above the threshold of 10.6, so the event is diagnosed as an inrush current.

E. Performance Evaluation Using Experimental Data

In this section, experimental data were used to evaluate the performance of the proposed method in the presence of experimental noise during data acquisition from a prototype transformer. The experimental circuit is as shown in Fig. 9. The experiments were carried out on a 6 kVA, 50 Hz, and 330 V/330 V power transformer. The transformer contains several access terminals to different points inside the windings. The internal faults are recorded practically by using these access terminals. More than 90 case studies in different situations are carried out and measured by a data logger with a sampling time equal to 128 microseconds.

Note that during experimental recording, the inrush and fault scenarios are recorded at no-load conditions. Due to lack of space, two of these scenarios are listed as follows:

1) Experimental inrush current

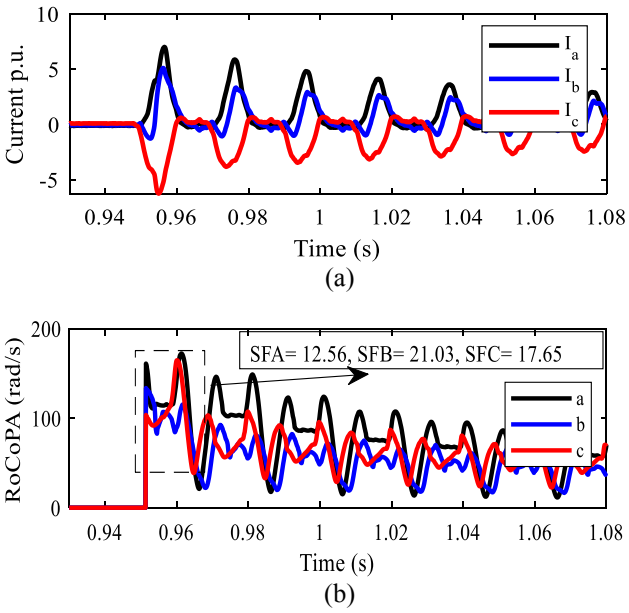

Fig. 10. Experimental circuit inrush current (a) Current, (b) RoCoPA.

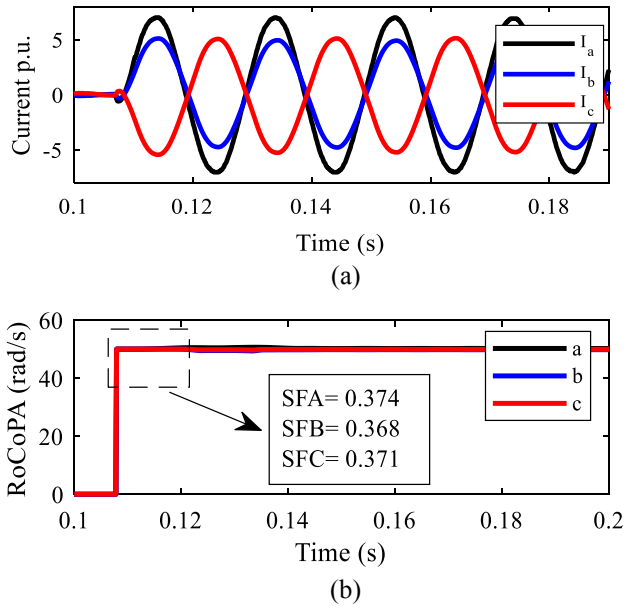

Fig. 11. Experimental fault current with no saturation (a) Current, (b) RoCoPA.

This scenario involves switching of the three-phase transformer, with a zero degree for phase c. The RoCoPA is shown in Fig. 10. By calculating its maximum standard deviation in the presence of experimental noise, a value greater than the threshold is obtained, so the event is correctly recognized as an inrush current is less than one cycle after transformer switching.

2) Experimental fault current

With the help of the experimental circuit, a scenario involving a three-phase fault is generated. As can be seen in Fig. 11, the three-phase current is slightly polluted by noise due to the measurement noise. By calculating the RoCoPA for all three phases and calculating its standard deviation, the maximum value of SFs is 0.374. This value is less than TH, which leads to the correct detection of the event as a fault. The delay of this scenario is 90 samples at the sampling frequency of 156 samples per

Table 4
Different Fault Scenarios.

Number of Scenarios	Fault from	to	Inception Time (ms)	Max (SF)	Number of Scenarios	Fault from	to	Inception Time (ms)	Max (SF)
1	a-10%	a- 40%-g	300	3.184	31	a-10%	a-40%	306	10.223
2	a-40%	g	300	3.111	32	a-60%	g	306	8.963
3	a-90%	g	300	3.045	33	a-10%	g	306	9.858
4	a-b	g	300	7.962	34	a-b-c	g	306	2.244
5*	a	g	300	1.310	35*	a	g	306	9.242
6	a-10%	g	300	2.883	36	a-10%	a-40%	306	8.535
7	a-40%	g	300	2.906	37	a-10%	g	306	7.981
8	a-90%	g	300	2.856	38	a-60%	g	306	8.180
9	a-b	g	300	8.120	39	a-b-c	g	306	8.320
10*	a	g	302	1.609	40*	a	b	306	8.500
11	a-10%	a-40%-g	302	1.113	41	a-10%	a-40%	308	10.027
12	a-40%	g	302	1.044	42	a-10%	g	308	9.139
13	a-90%	g	302	1.048	43	a-60%	g	308	8.751
14	a-b	g	302	2.816	44	a-b-c	g	308	5.853
15*	a	b	302	1.320	45*	a	g	308	9.611
16	a-10%	a-40%	302	1.342	46	a-10%	a-40%	308	8.705
17	a-40%	g	302	1.382	47	a-10%	g	308	8.639
18	a-90%	g	302	1.395	48	a-60%	g	308	8.944
19*	a-b	g	302	2.635	49	a-b-c	g	308	5.825
20	a-10%	g	304	1.584	50*	a	b	308	8.645
21	a-10%	a-40%-g	304	1.574	51	a-10%	a-40%	310	3.162
22	a-40%	g	304	1.714	52	a-10%	g	310	3.161
23	a-90%	g	304	1.591	53	a-60%	g	310	2.982
24*	a-b	g	304	3.558	54	a-b-c	g	310	1.552
25*	a	g	304	9.886	55*	a	g	310	3.018
26	a-10%	a-40%-g	304	2.266	56	a-10%	a-40%	310	2.873
27	a-40%	g	304	2.280	57	a-10%	g	310	2.928
28	a-90%	g	304	2.259	58	a-60%	g	310	2.766
29*	a-b	g	304	3.599	59*	a-b-c	g	310	8.943
30*	a	b	304	9.544	60*	a	b	310	10.223

Table 5
Different Inrush CURRENT SCENARIOS.

Number of Scenarios	Switching time (ms)	max (SF)	Number of Scenarios	Switching time (ms)	max (SF)
1	300	815.673	12	300	1645.848
2	301	2026.199	13	301	1654.499
3	302	1511.719	14	302	647.452
4	303	802.896	15	303	821.573
5	304	1911.386	16	304	1179.841
6	305	1559.011	17	305	1184.191
7	306	876.508	18	306	1849.152
8	307	12.097	19	307	1284.654
9	308	2043.793	20	308	1157.272
10	309	1066.595	21	309	1570.288
11	310	713.705	22	310	1645.848

Table 6
DIFFERENT INRUSH CURRENT with different Remanent flux.

Number of Scenarios	Switching time (ms)	Remanent Flux	max (SF)
1	300	−10%	145.248
2	300	30%	164.413
3	300	−70%	267.452
4	302	10%	921.473
5	302	−30%	179.741
6	302	70%	384.191
7	306	−10%	673.192
8	306	30%	384.654
9	306	−70%	1287.228
10	310	10%	770.458
11	310	−30%	1425.848
12	310	70%	193.458

cycle.

F. Discussion on the Simulation Results

So far, several scenarios have been described. Due to lack of space, the rest of the simulated cases will be as Tables 4, and 5. Table 4 contains the internal fault scenarios, and Table 5 contains the inrush current scenarios. Scenarios include faults with different inception angles and inrush current with different switching times and random noise levels with random SNR in the range of 30 dB to 50 dB.

In Table 5, 'g' means 'ground', 'a', 'b' and 'c' are three phases. For example, 'a-10%' and 'a-40%-g' mean 10% of phase coils and 40% of phase coils connected to the ground, respectively. Also, the star sign denotes the internal fault current, accompanied by CT saturation.

According to Table 4, the proposed method detects the internal transformer fault and the terminal fault with an appropriate distance from the TH. The proposed method can properly deal with internal fault current with CT saturation. As shown in Table 4, for the fault current with CT saturation, in the worst-case scenario (i.e., scenario 60), the discrimination index is less than the TH. Considering additive random noise in the fault current signal, the proposed method has been able to detect minor and major internal fault current with/without CT saturation with an acceptable distance from the TH.

Table 5 contains two types of transformers with conventional (scenarios 1 to 11) and modern (scenarios 12 to 22) core. It can be seen that in all the scenarios of Table 5, the inrush current is correctly recognized. It should be noted that modern core transformers have an upper knee-point comparing with conventional transformers. While modern core transformers impose difficulty for harmonic restrains-based algorithms,

Table 7
DIFFERENT INRUSH CURRENT with Internal fault SCENARIOS.

Number of Scenarios	Switching time (ms)	Fault Location	max (SF)
1	300	a-10%-g	9.648
2	300	a-20%-g	4.579
3	300	a-40%-g	7.982
4	302	a-10%-g	8.538
5	302	a-20%-g	4.836
6	302	a-40%-g	7.172
7	306	a-10%-g	10.152
8	306	a-20%-g	5.641
9	306	a-40%-g	7.372
10	310	a-10%-g	10.288
11	310	a-20%-g	8.008
12	310	a-40%-g	9.479

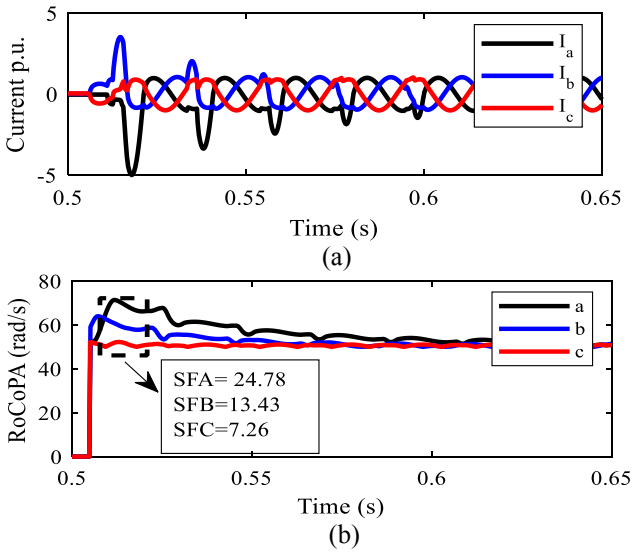

Fig. 12. Recovery inrush current (a) Current, (b) RoCoPA.

the proposed method successfully identifies inrush scenarios owning to RoCoPA variations in the inrush current signal. Table 6 shows the performance of the proposed method in the case of inrush currents with different remanent fluxes. As shown in Table 6, regardless of the polarity of the remanent flux, the proposed method shows high accuracy in detecting inrush currents. As a matter of fact, distortions in the inrush current with high remanent help more variations in RoCoPA, and as a result, the proposed method successfully identifies inrush current signals. Table 7 illustrates the performance evaluation of the proposed method for inrush current with an internal fault. As shown in Table 7, the proposed method can deal with the inrush current with an internal fault with the acceptable distance between the proposed criterion and TH. Due to dependency on the RoCoPA, the proposed method is able to detect the fault scenario even in the transformer energization condition.

G. Special Cases

In the following, some exceptional cases are investigated to evaluate the performance of the proposed method.

1) Recovery Inrush current

When a fault occurs, owning to transformer excitation decreasing, the voltage drops significantly. However, after fault clearance, due to the excitation of the transformer with recovery voltage, the inrush current is observed in the transformer. As a result, after fault clearance, the differential protection of the power transformer observes a large inrush with a shorter time compared with transformer energization. It is evident that the differential relay should not trip during recovery inrush. Note that the magnitude of the recovery inrush current is usually lower than the initial inrush case. However, the shape and harmonic profile of the recovery inrush current are similar to those measured during initial energizing.

Fig. 12 shows a sample recovery inrush current after external fault clearance. As it can be seen in Fig. 12, the maximum value of SF's is 24.78, and it is notably more significant than the threshold. As a result, the proposed algorithm can identify recovery inrush current in almost half a cycle.

2) Fault Current Limiter

Fault current limiters (FCLs) are employed to reduce the short circuit current level in the first cycle after fault occurrence. Regardless of the type of FCL, the presence of an FCL creates an abrupt change in the current and voltage waveforms. Such a waveform deformation may potentially threaten the performance of the differential protection. Here, the performance of the proposed method is evaluated under three types

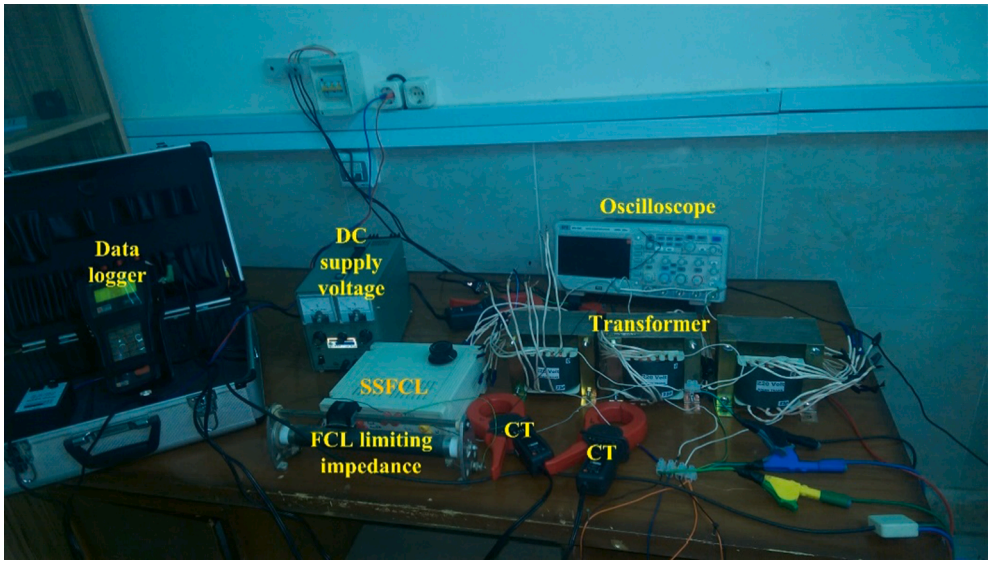

Fig. 13. Photo of a prototype transformer.

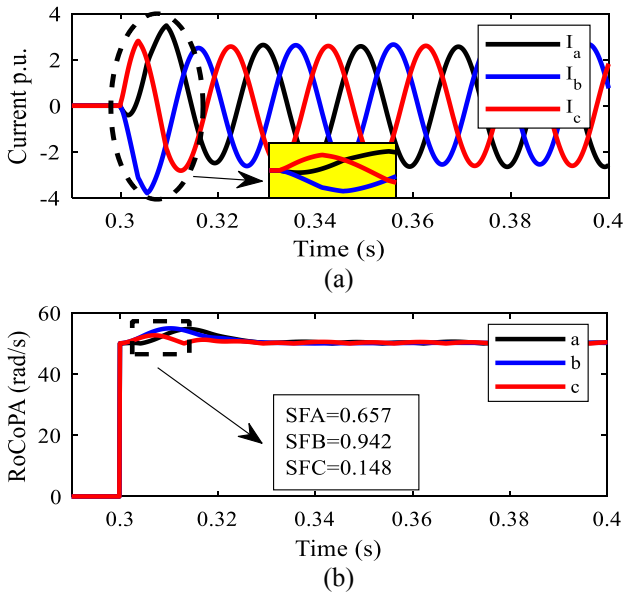

Fig. 14. Experimental fault current in the presence of R-FCL (a) Current, (b) RoCoPA.

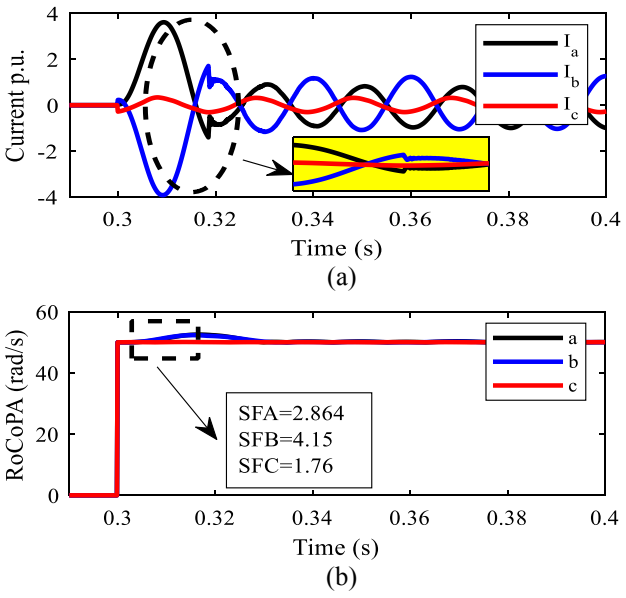

Fig. 16. Experimental fault current in the presence of SFCL (a) Current, (b) RoCoPA.

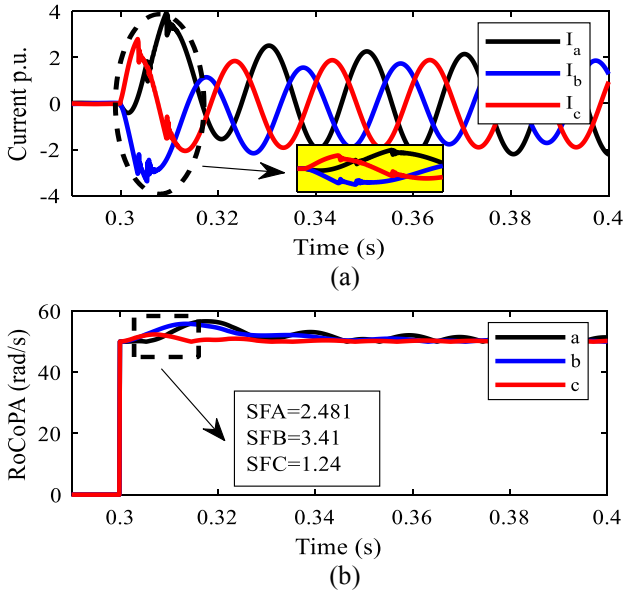

Fig. 15. Experimental fault current in the presence of L-FCL (a) Current, (b) RoCoPA.

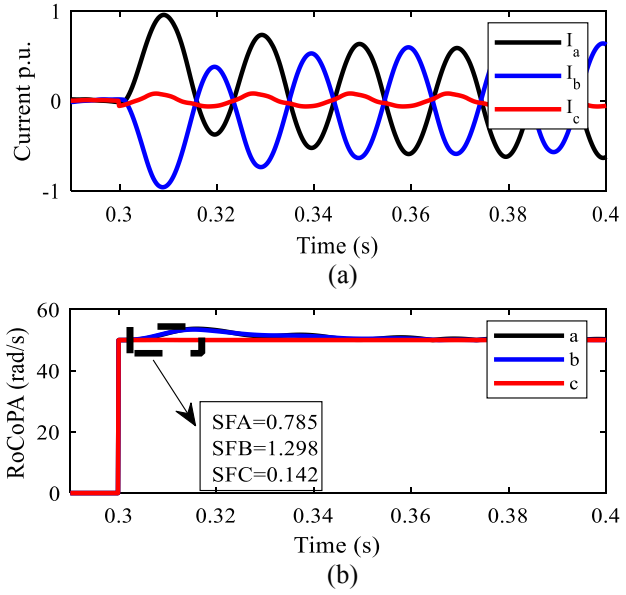

Fig. 17. Fault current in the presence of high impedance fault at transformer terminal (a) Current, (b) RoCoPA.

of FCLs, including resistive type FCL (R-FCL), inductive type FCL (L-FCL), and superconductive type of FCL (SSFCL). The characteristics of the FCLs are given from [17].

To obtain fault data in the presence of the FCL, the experimental setup, which is illustrated in Fig. 13, contains a power transformer with 3 kVA apparent nominal power. The power transformer operates at 50 Hz, with a voltage level of 220 / 380 V. The power transformer has various access terminals of the windings for applying internal faults. More than 100 inrush and internal faults in the presence of a different type of FCLs are generated and recorded considering 128 microseconds sampling time for the data logger.

According to Figs. 14 to 16, the proposed method is capable of detecting internal fault scenarios even considering waveform deformations due to the presence of the different types of FCLs. Note that maximum SF's for R-FCL, L-FCL, and SFCL are 0.924, 3.41, and 4.15, respectively, which confirm the higher deformation in the case L-FCL and SFCL will result in higher RoCoPA deviation. Nevertheless, in all cases, the maximum SF's is much lower than the threshold, which shows the reliability of the proposed index in the presence of the different types of FCLs.

3) High Impedance Fault in Transformer Terminal

In the following, the performance of the proposed method under high impedance fault in the transformer terminal is investigated. A single-phase fault at phase a with 10 Ω impedance is applied at t = 0.302 s. As indicated in Fig. 17, due to low variations of the RoCoPA with a maximum SF of about 1.298, the proposed method identifies the signal as a fault.

Considering the obtained results in Tables 5 and 7 and Figs. 4 and 17,

Table 8
Performance of the Proposed Method Considering Frequency Deviation during fault scenarios.

Number of Scenarios	Frequency Deviation (Hz)	Max (SF)
1	−1	6.894
2	−0.8	7.591
3	−0.6	7.067
4	−0.4	6.997
5	−0.2	7.151
6	0	7.088
7	0.2	7.913
8	0.4	7.068
9	0.8	7.594
10	1	6.746

Table 9
Comparison between Proposed Method and SHR method under DIFFERENT INRUSH CURRENT with different Remanent flux.

Number of Scenarios	Max (SF)	Time Delay	SHR%	Time Delay
1	145.248	11.52	19.92	41.945
2	164.413	11.52	21.92	36.28
3	267.452	11.52	20.05	38.002
4	921.473	11.52	24.49	38.054
5	179.741	11.52	17.04	37.985
6	384.191	11.52	23.58	36.162
7	673.192	11.52	17.15	37.668
8	384.654	11.52	21.1	39.746
9	1287.228	11.52	20.18	39.736
10	770.458	11.52	19.79	38.597
11	1425.848	11.52	18.09	38.643
12	193.458	11.52	21.24	41.594

Table 10
Comparison between Proposed Method and SHR method under DIFFERENT INRUSH CURRENT with Internal fault SCENARIOS.

Number of Scenarios	Max (SF)	Time Delay	SHR%	Time Delay
1	9.648	11.52	12.34	38.156
2	4.579	11.52	14.03	44.188
3	7.982	11.52	11.16	45.106
4	8.538	11.52	13.26	45.421
5	4.836	11.52	11.18	51.542
6	7.172	11.52	12.31	46.23
7	10.152	11.52	13.87	45.734
8	5.641	11.52	12.84	42.756
9	7.372	11.52	11.29	48.437
10	10.288	11.52	13.87	51.691
11	8.008	11.52	12.9	46.372
12	9.479	11.52	13.86	45.025

the proposed method can deal with a different type of internal fault with low and high impedances due to dependency on RoCoPA variation.

4) Deviation in the Frequency of the Fault Current Signal

Due to fault severity, the frequency may deviate from its nominal value in a real power grid. As a result, dealing with the off-nominal condition may become a challenge for numerical protective relays [31]. In the following, the proposed method's performance is evaluated for the fault scenario given in Fig. 5 under frequency variation.

As it can be seen in Table 8, frequency variation in the range of 49 to 51 Hz does not significantly affect the value of the maximum SF's. It should be noted that since the proposed algorithm depends on the variations of the RoCoPA, shifting in the frequency cannot notably affect the proposed criterion.

5) Comparison with Second Harmonic Restraint

Table 11
Performance Comparison Between References [19–21,25] and the Proposed Algorithm.

	[19]	[20]	[21]	[25]	Proposed Index
Requiring An extra index for CT saturation detection	No	No	No	Yes	No
Immune operation during CT saturation	Yes- with delay	Yes- with delay	Yes	Yes	Yes
Performance in the presence of FCL, off-nominal frequency	No	No	No	No	Yes
Required ideal data from current signal	1 Cycle	< ½ cycle	1 Cycle	¼ cycle	½ cycle
Range of operating time (OT) during different scenario	OT < 1 cycle	½ cycle < OT < 1 cycle	½ cycle < OT < 1 cycle	½ cycle < OT < 1 cycle	OT ≈ ½ cycle
Complexity	Medium	Medium	Low	High	Medium

In the following, the performance of the proposed method is compared with the second harmonic restrain method. The comparison is only conducted for hard cases given in Tables 5 and 6. Note that the threshold for the SHR method is adjusted to 15% [3,32].

As shown in Table 9, the proposed method, depending on the RoCoPA deviation, can identify the inrush scenarios in less than almost 12 ms. However, due to decreasing the second harmonic content in the presence of high remnant flux in the inrush current, the SHR method experiences a long delay of up to 42 ms.

For the given scenarios in Table 10, the proposed method can identify the internal faults in less than 12 ms. However, the SHR algorithm fails to detect the fault scenarios for almost 52 ms. The SHR fails during transformer energization with internal fault due to low second harmonic content. As a result, compared with the SHR method, the proposed algorithm has a remarkable speed of convergence incorrect recognition of the scenarios.

H. Comparing Proposed Method with State-of-the-Art

Performance comparison is conducted qualitatively in Table 1 and a quantitative manner with the SHR algorithm in Section 3, subsection G, part 5. In general, the proposed method belongs to hybrid, and innovative algorithms that have more flexibility than other groups of algorithms are given in Table 1. However, to compare with some of the most recent algorithms of hybrid and innovative algorithms (A5) according to Table 1 with the proposed algorithm, the following comparison is provided.

- According to Table 11, unlike Ref. [25], the other methods do not require extra CT saturation detection algorithms. Also, all algorithms have a good performance during CT saturation, and the differences are in the time delays.
- Refs. [19–21] and [25] are based on waveform similarity index that suffers from off-nominal frequency condition and waveform deformation in the case of the presence of FCL in the neutral transformer. While the proposed method robustly can deal with the latter conditions without compromising the operating time.
- Refs. [19] Moreover, [20] require one cycle and half-cycle data for performing calculations, respectively. Ref. [21] requires one cycle current signal for normalizing the current signal, and afterward, it employs a quarter cycle to calculates its index. Eventually, Ref. [25] requires only a quarter cycle of the current signal. Comparing with

Table 12
Average Operating Time of Refs. [19–21,25] and the Proposed Algorithm (OTs are in ms).

Scenarios	[19]	[20]	[21]	[25]	Proposed Index
Inrush	18.96	14.24	14.52	13.1	11.52
Internal Fault	20.42	12.98	15.67	12.06	11.52

these algorithms, the proposed index requires up to half-cycle data for performing the evaluation.

- The range of operating time (OT) during different scenarios for Ref. [19] is less than one cycle. The range of OT in Refs. [20], [21] and [25] are less than one cycle. However, the OT range in the proposed method is a fixed value, and it is about half-cycle. Combining with the previous point (point 3), the proposed method has supremacy both in requiring the lowest data and response time comparing with the other methods.
- Eventually, while the Ref. [21] has the lowest complexity, considering all of the challenges given in Table 11, it seems the proposed index provides more flexibility and reliability in discrimination of internal fault and inrush current with good accuracy and fast response.

To compare the performance of the proposed algorithm with the methods in [19–21,25], several scenarios, including 1000 inrush currents and 1000 internal fault current scenarios, are applied to the algorithms. The inrush scenarios are generated with high-remanent flux in the range of (-80% to 80%). Also, the internal fault scenarios are accompanied mainly by CT saturation. Table 12 shows the results of the algorithms in which the algorithms have succeeded in correctly identified scenarios. The results in Table 12 indicate that the proposed method has the lowest OTs among the algorithms.

Overall comparison between the proposed algorithm with the methods in [19–21,25] in Tables XI and XII reveal that the proposed algorithm provides good accuracy and response time comparing with the other algorithms.

4. Conclusion

Quick and reliable internal fault and inrush current discrimination enhances the reliable operation of differential protection of the power transformers. A RoCoPA-based algorithm for discrimination of internal fault and inrush currents of the power transformer was presented in this paper. Owning to a standard power system signal (i.e., a sinusoidal waveform), the RoCoPA shows low variations during the fault. However, magnetization inrush current has RoCoPA with high fluctuation. Based on the simulated and experimental data, the performance of the proposed algorithm was evaluated under various internal fault and inrush currents. It has been observed that the proposed algorithm successfully identifies internal fault signals even in the case of minor internal turn-to-turn fault signal, internal fault accompanied with CT saturation, and internal fault during inrush current. Also, the performance of the proposed algorithm during various inrush current cases indicates that the proposed index can clearly recognize inrush current from the internal fault signal. The simulation results show that the proposed method has good immunity against noise, source frequency variation, decaying DC component. Compared with the second harmonic restrain method, the proposed algorithm shows high accuracy and fast response. While SFCL may distort the fault signal in the first quarter of the cycle, the proposed algorithm shows immunity against such distortion. It can successfully discriminate the fault signal even in the presence of SFCL. Being independent of transformer parameters, performance evaluation on both simulation and experimental data indicate the threshold of this paper can be easily employed for the different test system. Considering the almost half-cycle delay in decision making in different challenging circumstances, the proposed method shows the ability and applicability for the internal fault and inrush currents discrimination. This paper aims to propose the concept of rate of change of phase angle to discriminate the internal fault from inrush current. However, future work can be dedicated to finding a lower complicated algorithm than LMS to reduce the computational burden.

Table 13
Power Transformer Saturation Curve

I (% of rated current)	V (per unit)
0	0
0.4	0.43
0.7	0.56
1.39	0.67
1.67	0.77
4.2	0.89
5.65	1
7.6	1.1
15.2	1.22
25	1.34

Table 14
HV side CT Saturation Curve

I (A(	E (V)
0.002	1
0.006	5
0.008	10
0.015	20
0.018	30
0.04	100
0.05	150
0.07	200
0.1	220
5	300

Table 15
LV side CT Saturation Curve

I (A(	E (V)
0.001	1
0.0028	5
0.0045	10
0.008	30
0.02	100
0.03	200
0.045	300
0.2	400
10	490
20	500

Declaration of Competing Interest

The authors declare that they have no known competing financial interests or personal relationships that could have appeared to influence the work reported in this paper.

Appendix A

The saturation curve of the simulated power transformer and its corresponding CTs is presented in Tables 13–15. The parameters of the 50 Hz simulated power systems, which is shown in Fig. 3, are as follows:

Source 1: $V_{rated} = 400$ kV, $R_{th1} = 2(\Omega)$, $L_{th1} = 0.064$(H).
Source 2: $V_{rated} = 230$ kV, $R_{th2} = 1.3(\Omega)$, $L_{th2} = 0.042$(H).

Line 1:

Positive Sequence Resistance $R_{L1} = 6.18 \times 10^{-3}\Omega$/km;
Zero Sequence Resistance $R_{0,\,L1} = 5.447 \times 10^{-2}\Omega$/km;

Positive Sequence Reactance $X_{L1} = 6.24 \times 10^{-3}\Omega$/km;
Zero Sequence Resistance $X_{0,\ L1} = 0.168\ \Omega$/km;
Positive Sequence Capacitance $C_{L1} = 0.0179\mu$F/km;
Zero Sequence Capacitance $C_{0,\ L1} = 0.0109\mu$F/km.

Line2:

Positive Sequence Resistance $R_{L2} = 0.\ 0544\ \Omega$/km;
Zero Sequence Resistance $R_{0,\ L2} = 0.2473\ \Omega$/km;
Positive Sequence Reactance $X_{L2} = 0.321\ \Omega$/km;
Zero Sequence Resistance $X_{0,\ L2} = 0.887\ \Omega$/km;
Positive Sequence Capacitance $C_{L2} = 0.0035\mu$F/km;
Zero Sequence Capacitance $C_{0,\ L2} = 0.0021\mu$F/km.

Transformer:

S_{rated} = 500MVA, 400/230 kV, Y–Δ connection.

HV side CT:

CT Ratio: 1200: 5, $R_{CT2} = 0.61\ \Omega$, $L_{CT2} = 9 \times 10$–4H.

LV side CT:

CT Ratio: 1200: 5, $R_{CT2} = 0.53\ \Omega$, $L_{CT2} = 7.8 \times 10$–4H.

References

[1] Bagheri S, Moravej Z, Gharehpetian GB. Classification and discrimination among winding mechanical defects, internal and external electrical faults, and inrush current of transformer. IEEE Trans Ind Inf 2018;14(2):484–93.
[2] Ni H, Fang S, Lin H. A Simplified Phase-Controlled Switching Strategy for Inrush Current Reduction. IEEE Trans Power Delivery Feb. 2021;36(1):215–22. https://doi.org/10.1109/TPWRD.2020.2984234.
[3] Golshan MH, Saghaian-Nejad M, Saha A, Samet H. A new method for recognizing internal faults from inrush current conditions in digital differential protection of power transformers. Electr Power Syst Res 2004;71(1):61–71.
[4] Zhang W, Tan Q, Mian S, Zhou L, Liu P. Self-adaptive transformer differential protection. Proc. Inst. Eng. Technol. Gen. Transm. Distrib. 2013;7(1):61–8.
[5] Phadke A, Thorp J. A new computer-based flux-restrained current-differential relay for power transformer protection. IEEE Transactions on Power Apparatus and Systems 1983;11:3624–9.
[6] Kang Y, Lee B, Kang S. Transformer protection relay based on the induced voltages. Int. J. Elect. Power Energy Syst. 2007;29(4):281–9.
[7] F. Haghjoo, M. Mostafaei, Flux-based turn-to-turn fault protection for power transformers, IET Gener. Transm. Distrib. 10 (2016) 1154–1163, https://doi.org/10.1049/iet-gtd.2015.0738.
[8] Periz LD, Flechsig AJ, Meador JL, Obradovic Z. Training an artificial neural network to discriminate between magnetizing inrush and internal faults. IEEE Trans. Power Del. Jan. 1994;9(1):434–41.
[9] Rahmati A, Sanaye-Pasand M. Protection of power transformer using multi criteria decision-making. Int. J. Elect. Power Energy Syst. Jun. 2015;68:294–303.
[10] S. Afrasiabi, M. Afrasiabi, B. Parang and M. Mohammadi, "Integration of Accelerated Deep Neural Network into Power Transformer Differential Protection," in IEEE Transactions on Industrial Informatics. doi: 10.1109/TII.2019.2929744.
[11] Guillén D, Esponda H, Vázquez E, Idárraga-Ospina G. Algorithm for transformer differential protection based on wavelet correlation modes. IET Gener. Transm. Distrib. Sep. 2016;10(12):2871–9.
[12] Medeiros RP, Costa FB. A wavelet-based transformer differential protection with differential current transformer saturation and cross-country fault detection. IEEE Trans. Power Del. Apr 2018;33(2):789–99.
[13] Rasoulpoor M, Banejad M. A correlation based method for discrimination between inrush and short circuit currents in differential protection of power transformer using discrete wavelet transform: Theory simulation and experimental validation. Int. J. Elect. Power Energy Syst. Oct. 2013;51:168–77.
[14] A. Roy, D. Singh, R. K. Misra and A. Singh, "Differential protection scheme for power transformers using matched wavelets," in IET Generation, Transmission & Distribution, vol. 13, no. 12, pp. 2423-2437, 18 6 2019.
[15] Sahebi A, Samet H, Ghanbari T. Identifying internal fault from magnetizing conditions in power transformer using the cascaded implementation of wavelet transform and empirical mode decomposition. International Transactions on Electrical Energy Systems 2018:2485.
[16] Sahebi A, Samet H. Efficient method for discrimination between inrush current and internal faults in power transformers based on the non-saturation zone. IET Gener Transm Distrib 2017;11(6):1486–93.
[17] A. Sahebi and H. Samet, "Discrimination between internal fault and magnetising inrush currents of power transformers in the presence of a superconducting fault current limiter applied to the neutral point," in IET Science, Measurement & Technology, vol. 10, no. 5, pp. 537-544, 8 2016.
[18] M. Ahmadi, H. Samet and T. Ghanbari, "Discrimination of internal fault from magnetising inrush current in power transformers based on sine-wave least-squares curve fitting method," in IET Science, Measurement & Technology, vol. 9, no. 1, pp. 73-84, 1 2015.
[19] A. Bagheri, M. Allahbakhshi, H. Samet, M. Tajdinian and A. Seifi, "Distinguishing between Fault and Inrush Current in Presence of the CT Saturation: a New Method Based on Gravity Center in Time," 2019 IEEE International Conference on Environment and Electrical Engineering and 2019 IEEE Industrial and Commercial Power Systems Europe (EEEIC / I&CPS Europe), Genova, Italy, 2019, pp. 1-5.
[20] Weng H, Wang S, Lin X, Li Z, Huang J. A novel criterion applicable to transformer differential protection based on waveform sinusoidal similarity identification. Int. J. Electr. Power Energy Syst. Feb. 2019;105:305–14.
[21] Zhang L, Wu QH, Ji TY, et al. Identification of inrush currents in power transformers based on high-order statistics. Electr. Power Syst. Res. 2017;146:161–3.
[22] M. Tajdinian, A. Bagheri, M. Allahbakhshi and A. R. Seifi, "Framework for current transformer saturation detection and waveform reconstruction," in IET Generation, Transmission & Distribution, vol. 12, no. 13, pp. 3167-3176, 31 7 2018.
[23] Ali E, Helal A, Desouki H, Shebl K, Abdelkader S, Malik O. Power transformer differential protection using current and voltage ratios. Electr Power Syst Res 2018;154:140–50.
[24] Perez M, Silva Kleber M. Power transformer protection using an instantaneous-current-value negative sequence differential element. Int. J. Electr. Power Energy Syst., Jun. 2019;108:96–106.
[25] F. Naseri, H. Samet, T. Ghanbari and E. Farjah, "Power transformer differential protection based on least squares algorithm with extended kernel," in IET Science, Measurement & Technology, vol. 13, no. 8, pp. 1102-1110, 10 2019.
[26] N. Chiesa, Power transformer modeling for inrush current calculation, 2009.
[27] Kwong Raymond H, Johnston Edward W. A variable step size LMS algorithm. IEEE Trans Signal Process 1992;40(7):1633–42.
[28] Huang Zhi-Kai, Chau Kwok-Wing. A new image thresholding method based on Gaussian mixture model. Appl Math Comput 2008;205(2):899–907.
[29] Moulin Pierre, Liu Juan. Analysis of multi resolution image denoising schemes using generalized Gaussian and complexity priors. IEEE Trans Inf Theory 1999;45(3):909–19.
[30] Otsu Nobuyuki. A threshold selection method from gray-level histograms. Automatica 1975;11(285–296):23–7.
[31] Tajdinian Mohsen, Jahromi Mehdi Zareian, Mohseni Kazem, Kouhsari Shahram Montaser. An analytical approach for removal of decaying DC component considering frequency deviation. Electr Power Syst Res 2016;130:208–19.
[32] Ghanbari Teymoor, Samet Haidar, Ghafourifard Javad. New approach to improve sensitivity of differential and restricted earth fault protections for industrial transformers. IET Gener Transm Distrib 2016;10(6):1486–94.